*J. Fluid Mech.* (2017), *vol.* 829, *pp.* 280–303.  
doi:10.1017/jfm.2017.536

# Radiation of internal waves from groups of surface gravity waves

**S. Haney**[1,†] **and W. R. Young**[1]

[1]Scripps Institution of Oceanography, UC San Diego, La Jolla, CA 90237, USA

(Received 30 January 2017; revised 29 July 2017; accepted 30 July 2017;
first published online 15 September 2017)

Groups of surface gravity waves induce horizontally varying Stokes drift that drives convergence of water ahead of the group and divergence behind. The mass flux divergence associated with spatially variable Stokes drift pumps water downwards in front of the group and upwards in the rear. This 'Stokes pumping' creates a deep Eulerian return flow that sets the isopycnals below the wave group in motion and generates a trailing wake of internal gravity waves. We compute the energy flux from surface to internal waves by finding solutions of the wave-averaged Boussinesq equations in two and three dimensions forced by Stokes pumping at the surface. The two-dimensional (2-D) case is distinct from the 3-D case in that the stratification must be very strong, or the surface waves very slow for any internal wave (IW) radiation at all. On the other hand, in three dimensions, IW radiation always occurs, but with a larger energy flux as the stratification and surface wave (SW) amplitude increase or as the SW period is shorter. Specifically, the energy flux from SWs to IWs varies as the fourth power of the SW amplitude and of the buoyancy frequency, and is inversely proportional to the fifth power of the SW period. Using parameters typical of short period swell (e.g. 8 s SW period with 1 m amplitude) we find that the energy flux is small compared to both the total energy in a typical SW group and compared to the total IW energy. Therefore this coupling between SWs and IWs is not a significant sink of energy for the SWs nor a source for IWs. In an extreme case (e.g. 4 m amplitude 20 s period SWs) this coupling is a significant source of energy for IWs with frequency close to the buoyancy frequency.

**Key words:** internal waves, stratified flows, surface gravity waves

## 1. Introduction

Surface gravity waves induce a horizontal Lagrangian mass flux known as the Stokes drift. The Stokes drift is proportional to the square of the amplitude of the waves and thus a slowly varying wave group has a spatially variable horizontal mass transport. The Stokes drift vanishes, as the waves do, at the edges of the group, thereby inducing a horizontal divergence of the vertically integrated Lagrangian transport. The converging Lagrangian mass flux at the front of the group drives water downward, while divergent Lagrangian mass flux at the rear of the group

† Email address for correspondence: shaney@ucsd.edu

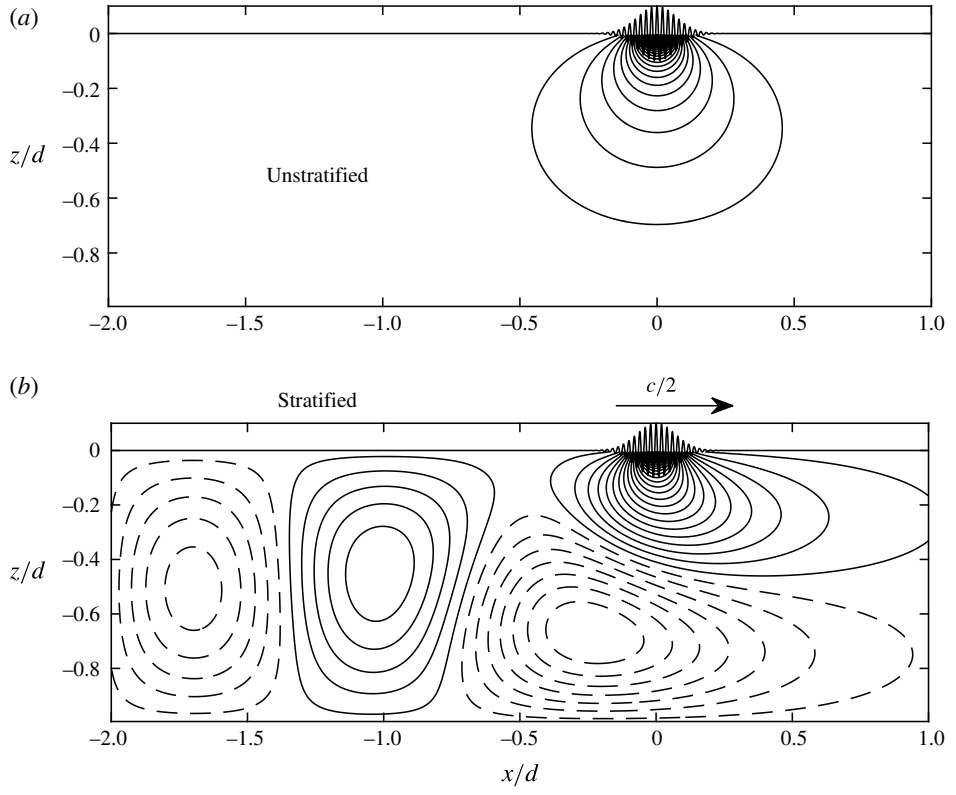


FIGURE 1. (*a*) The streamfunction of the deep return flow beneath the Gaussian SW group in (A 1) with an unstratified interior. (*b*) Constant $N = 7 \times 10^{-3}$ s$^{-1}$. The dashed contours indicate negative values of the streamfunction, and the contour interval is 0.05 m$^2$ s$^{-1}$. In both panels, the SW group is moving to the right with group speed $c/2$ with $c = \sqrt{g/k}$. The SW amplitude is exaggerated by orders of magnitude in order to visualize the group; in this illustration of a 'two-dimensional' group $\ell_x/d = 0.07$ and $\ell_y = \infty$ where $\ell_x$ and $\ell_y$ are the horizontal length scales of the Gaussian packet in (A 1).

lifts it up. This 'Stokes pumping' drives a deep Eulerian return flow, first shown by Longuet-Higgins & Stewart (1964), discussed further by McIntyre (1981) and van den Bremer & Taylor (2015) and depicted in figure 1(*a*).

The deep return flow beneath a surface wave (SW) group in an unstratified fluid is shown in figure 1(*a*). The positive momentum contained in the vertically integrated Stokes drift is balanced by the momentum in the deep Eulerian return flow so that the total momentum in a large volume is zero (McIntyre 1981). The structure of the deep return flow can be understood with an electrostatic analogy in which the streamlines are lines of force induced by the dipolar Stokes pumping, essentially at the surface $z = 0$. Consequently, in the two-dimensional (2-D) case, the velocity of the deep return flow decays slowly with depth, $z$, as $z^{-2}$ below the group so that the bottom at $z = -d$ has important effects even in very deep water. In the three-dimensional (3-D) case, some of the return flow may go around rather than underneath the SWs. Thus in the 3-D case the decay of deep currents is faster, but still algebraic as $z^{-3}$ (van den Bremer & Taylor 2015).

Here we investigate the effects of stratification on the structure of the Eulerian mean return flow beneath a group of SWs. As anticipated by McIntyre (1981), stable stratification greatly modifies the form of the return flow by exciting internal gravity waves as the SW group passes above: see figure 1(*b*).

To make a direct comparison with the unstratified return flow in figure 1(*a*) we have also shown the streamfunction in figure 1(*b*). However, with typical oceanic stratification, the 2-D and 3-D situations are strikingly different. In the 2-D case, the phase speed of the internal waves (IWs) is necessarily in the same direction as that of SW propagation: in figure 1(*b*) the $x$-phase speed of the IW train is equal to the SW group velocity, $c/2$ with $c = \sqrt{g/k}$. The group speed of swell with typical wavelengths of 100 m or greater exceeds 5 m s$^{-1}$. But Chelton *et al.* (1998) show that the IW phase speed in the ocean never exceeds 3.2 m s$^{-1}$. Thus the radiation of IWs by strictly two-dimensional SWs – the situation shown in figure 1(*b*) – does not occur in Earth's ocean. In other words, ocean stratification is so weak that in the 2-D case IWs cannot keep up with swell and there is no radiation. But in the 3-D case, in which the SW packet has finite extent in the spanwise ($y$) direction, radiated IWs can propagate obliquely to the direction of propagation (the $x$-axis) of the SW group. With oblique propagation the phase speed of IWs along the $x$-axis can equal $c/2$ even in a weakly stratified ocean. Thus IW radiation from SW groups is much more efficient in three than in two dimensions.

The coupling of SWs and IWs has been explored previously in oceanography as a possible mechanism for energizing the ocean IW field. The recent paper by Olbers & Eden (2016) reviews this oceanographic literature, starting with the first estimates of the strength of SW driving of IWs (Watson, West & Cohen 1976; Olbers & Herterich 1979). These estimates are based on resonant triad theory and employ a spectral characterization of the SW field. But resonant triad theory does not directly reveal the effect of stratification on the situation in figure 1(*b*) in which the deep return flow associated with a narrow-band group of ocean swell shakes the deep, stable stratification of the ocean.

However there is a connection between IW radiation from the SW group in figure 1(*b*) and resonant triad theory: radiation of IWs requires that the phase speed of the IW must match the speed of the forcing, which is the group speed of the SWs. This condition is a special case of triad resonance in which the SW group constitutes two members of the triad with close wavenumbers $k$ and $k + \delta k$, and the radiated IW is the third member of the triad with wavenumber $\delta k \ll k$. In this paper we are isolating this particular triad interaction as it applies directly to situation in figure 1(*b*) and showing the connection to Stokes drift and the associated deep return flow.

In § 2 we recall the first order in wave amplitude solution in terms of the standard velocity potential; considering the second order in wave amplitude, we perform a phase average to obtain the IW equation forced by the divergence of the mean wave momentum at the surface. In § 3 we solve the surface forced IW equation to obtain the wave-averaged vertical velocity and pressure. In § 4 we obtain an expression for the energy flux from SWs to IWs; we show that our estimate of energy flux is in quantitative agreement with the resonant triad estimate of Olbers & Eden (2016). In § 5 we discuss the 2-D limit of the 3-D energy flux solution. Section 6 is the discussion and conclusion.

## 2. Formulation

We decompose the density as

$$\rho = \rho_0 \left[ 1 + \frac{1}{g} \left( \int_z^0 N^2(z')\, \mathrm{d}z' - b \right) \right], \tag{2.1}$$

where $\rho_0$ is the average density, $g$ is the gravitational acceleration acting in the negative $z$-direction, $N^2(z)$ is the buoyancy frequency and $b(x, y, z, t)$ is the buoyancy (e.g. Phillips 1977). The Boussinesq equations are

$$\boldsymbol{u}_t + \boldsymbol{u} \cdot \boldsymbol{\nabla} \boldsymbol{u} + \boldsymbol{\nabla} p = b\hat{\boldsymbol{z}}, \tag{2.2}$$

$$b_t + \boldsymbol{u} \cdot \boldsymbol{\nabla} b + wN^2 = 0, \tag{2.3}$$

$$\boldsymbol{\nabla} \cdot \boldsymbol{u} = 0, \tag{2.4}$$

where the velocity is $\boldsymbol{u} = u\hat{\boldsymbol{x}} + v\hat{\boldsymbol{y}} + w\hat{\boldsymbol{z}}$ and $p$ is the non-hydrostatic constituent of the pressure divided by the average density $\rho_0$.

We denote the magnitude of the free-surface displacement by $a_{max}$, the wavenumber of the primary SW by $k$ and the horizontal length scale of the SW group in the $x$-direction by $\ell_x$. Using these scales the wave steepness and scale separation parameters are

$$\epsilon \stackrel{\text{def}}{=} a_{max} k, \quad \text{and} \quad \mu \stackrel{\text{def}}{=} \frac{1}{k\ell_x}. \tag{2.5a,b}$$

We assume that $\epsilon$ and $\mu$ are both small and we neglect the direct effects of stratification in the shallow wave zone where $kz$ is order one. This assumption is justified provided that the wave frequency $\sqrt{gk}$ is much greater than $N(z)$ in this region. In the along-crest ($y$) direction, the SW group has length $\ell_y$; we treat $\ell_y/\ell_x$ as order one.

Denoting the free-surface displacement by $h(x, y, t)$, the surface boundary conditions, correct to second order in wave steepness $\epsilon$, are

$$\text{at } z = 0: \quad h_t + (uh)_x + (vh)_y = w, \tag{2.6}$$

and

$$\text{at } z = 0: \quad p + hp_z = gh + N^2 \tfrac{1}{2} h^2, \tag{2.7}$$

where $(\,)_x$ indicates an $x$-derivative, and similarly for $y$, $z$, and $t$ derivatives. In (2.6) and (2.7) we have transferred the surface boundary conditions from the moving free surface $z = h$ to the flat surface $z = 0$ using the Stokes expansion. The bottom boundary condition is $w(x, y, -d, t) = 0$. We confine attention to deep water waves, $kd \gg 1$, so that the bottom boundary condition is important only for the deep return flow beneath the SW group.

Scaling time with the wave frequency $\sqrt{gk}$ and length with the wavenumber $k$ sets $g \to 1$. One then expands all variables in powers of wave steepness $\epsilon$; for example

$$p = \epsilon p_1 + \epsilon^2 p_2 + \cdots. \tag{2.8}$$

While we are guided by this scheme when choosing to neglect or retain terms, for clarity we develop the expansion using the original dimensional variables.

### 2.1. *The solution at first order*

In the first-order equations we neglect the small buoyancy force $b_1\hat{\boldsymbol{z}}$ on the right of the momentum equation (2.2). With this approximation the classic first-order solution is irrotational and is expressed using the familiar velocity potential $\phi(x, y, z, t)$:

$$\boldsymbol{u}_1 = \boldsymbol{\nabla}\phi, \quad \text{and} \quad p_1 = -\phi_t. \tag{2.9a,b}$$

The problem then reduces to the solution of the 3-D Laplace equation $\phi_{xx} + \phi_{yy} + \phi_{zz} = 0$ with the surface boundary condition $\phi_{tt} + g\phi_z = 0$ at $z = 0$ and the deep water condition that $\phi(x, y, -\infty, t) = 0$. Correct to leading order in the scale separation parameter $\mu$, the first-order solution for an SW group is

$$h_1 = \tfrac{1}{2}a(\tilde{x}, y, 0)\exp[\mathrm{i}k(x - ct)] + \text{c.c.}, \tag{2.10}$$

$$\phi = -\tfrac{1}{2}\mathrm{i}ca(\tilde{x}, y, z)\exp[\mathrm{i}k(x - ct) + kz] + \text{c.c.}, \tag{2.11}$$

where $a(\tilde{x}, y, z)$ is the slowly varying envelope, $c = \sqrt{g/k}$ is the SW phase speed, c.c. denotes the complex conjugate, and

$$\tilde{x} \overset{\text{def}}{=} x - \tfrac{1}{2}ct, \tag{2.12}$$

is the wave group coordinate; $c/2$ in (2.12) is the deep water group velocity. We neglect dispersive spreading of the group (see van den Bremer & Taylor 2016).

### 2.2. *Quadratic properties of the first-order solution*

At next order we need several quadratic properties of the first-order solution, some of which are expressed most easily using the first-order wave displacement $\boldsymbol{\xi}_1$ defined via

$$\boldsymbol{\xi}_{1t} = \boldsymbol{u}_1 = \boldsymbol{\nabla}\phi. \tag{2.13}$$

At $z = 0$ the vertical displacement $\zeta_1(x, y, z, t) = \hat{\boldsymbol{z}} \cdot \boldsymbol{\xi}_1$ is the same as the first-order displacement of the free surface $h_1(x, y, t)$; the dynamically negligible buoyancy perturbation in the wave zone is diagnosed as $b_1 = -N^2\zeta_1$.

Denoting a running phase average over the fast oscillation of the primary wave by an overbar, the Stokes drift in the $x$-direction is

$$u^S \overset{\text{def}}{=} \overline{\boldsymbol{\xi}_1 \cdot \boldsymbol{\nabla} u_1} = ck^2|a|^2\mathrm{e}^{2kz}. \tag{2.14}$$

The mean wave momentum per unit area in the $x$-direction is $\rho_0 M$, where

$$M \overset{\text{def}}{=} \overline{u_1\zeta_1}|_0 = \tfrac{1}{2}ck|a|^2, \tag{2.15}$$

with $|_0$ indicating evaluation at $z = 0$. The identity

$$M = \int_{-\infty}^{0} u^S \,\mathrm{d}z \tag{2.16}$$

shows that $u^S$ can be interpreted as the vertical distribution of the mean wave momentum (e.g. Phillips 1977). The chain of identities

$$\overline{\zeta_1 p_{1z}} = -\overline{\zeta_1 w_{1t}} = \overline{w_1^2} = \tfrac{1}{2}\overline{|\boldsymbol{u}_1|^2} = \tfrac{1}{2}cu^S \tag{2.17}$$

is useful at next order. The identities in (2.17) express all important wave-averaged quantities in terms of the Stokes drift in (2.14).

### 2.3. *The second-order wave-averaged equations of motion*

To write the phase-averaged second-order equations compactly we introduce the Bernoulli function

$$\varpi \overset{\text{def}}{=} \bar{p}_2 + \tfrac{1}{2}\overline{|\boldsymbol{u}_1|^2}. \tag{2.18}$$

Using $\varpi$, the phase-averaged second-order equations are

$$\bar{\boldsymbol{u}}_{2t} + \boldsymbol{\nabla}\varpi = \bar{b}_2\hat{\boldsymbol{z}}, \tag{2.19}$$

$$\bar{b}_{2t} + \overline{w}_2 N^2 = 0, \tag{2.20}$$

$$\boldsymbol{\nabla}\cdot\bar{\boldsymbol{u}}_2 = 0. \tag{2.21}$$

We have neglected the term $\boldsymbol{u}_1\cdot\boldsymbol{\nabla}b_1$ in (2.20) because this term decays exponentially with depth over a layer of depth $(2k)^{-1}$. This term is important for mixed layer dynamics, but not for the deep return flow or wake of radiated IWs. Although the buoyancy force $b\hat{\boldsymbol{z}}$ has a negligible effect on the SW group it does affect the deep flow and therefore it is essential to retain $\bar{b}_2\hat{\boldsymbol{z}}$ in (2.19). Because of the buoyancy force, the deep flow beneath the SW group is not irrotational and thus it is not possible to use a velocity potential to represent the solution of (2.19)–(2.21). Instead the system can be combined to obtain the IW equation for the second-order wave-averaged vertical velocity

$$[\partial_t^2(\partial_x^2+\partial_y^2+\partial_z^2)+N^2(\partial_x^2+\partial_y^2)]\bar{w}_2 = 0. \tag{2.22}$$

Combining (2.20) with the vertical part of (2.19), the pressure $\varpi$ can be expressed in terms of the second-order vertical velocity as

$$\varpi_{zt} = -(\partial_t^2 + N^2)\bar{w}_2. \tag{2.23}$$

The wave-averaged second-order surface boundary conditions following from (2.6) and (2.7) are

$$\text{at } z=0: \quad \bar{h}_{2t} + M_x = \overline{w}_2, \tag{2.24}$$

and

$$\text{at } z=0: \quad \varpi = g\bar{h}_2 + N^2\tfrac{1}{2}\overline{h_1^2}. \tag{2.25}$$

Identity (2.17) has been used to express the surface boundary condition (2.25) in terms of $\varpi$. Following earlier authors (e.g. Longuet-Higgins & Stewart 1964; van den Bremer & Taylor 2015), we make the 'rigid-lid approximation' by neglecting $\bar{h}_{2t}$ in (2.24) so that the surface boundary condition simplifies to

$$\text{at } z=0: \quad \bar{w}_2 \approx M_x. \tag{2.26}$$

Note that neglecting the mean sea surface displacement, $\bar{h}_2$, is only valid in deep water (see van den Bremer & Taylor 2015). If required, the mean surface displacement $\bar{h}_2$ can be diagnosed from (2.25) as $\bar{h}_2 \approx g^{-1}\varpi|_0$. The bottom boundary condition is $\bar{w}_2 = 0$.

## 3. Radiating solutions of the second-order wave-averaged equations

Solving the IW equation (2.22) for $\bar{w}_2$, we encounter a well-known issue in radiation problems: there are zero denominators related to the resonance condition that the IW phase speed in the $x$-direction must be equal to the SW group speed $c/2$. The physical resolution of this mathematical problem is the correct application of the causality condition, also known as the Sommerfeld radiation condition, that the internal gravity waves are outgoing from the SW packet. To implement the Sommerfeld condition, we follow the method of Lighthill (1967, 1978) and assume that the SW group has been growing very slowly from $t=-\infty$ at a rate $\delta$. The quasi-steady solution is found by taking the limit $\delta \to 0$ though positive real values. Thus the boundary condition (2.26) is modified to

$$\text{at } z=0: \quad \bar{w}_2 = \mathrm{e}^{\delta t} M_x, \tag{3.1}$$

with $\delta > 0$.

### 3.1. *Projection onto vertical modes and Fourier transform*

With uniform $N$ we express the solution of the IW equation (2.22) and the pressure equation (2.23) as a sum of orthonormal vertical modes:

$$\bar{w}_2 = \sum_{n=1}^{\infty} w_n(x, y, t)\sqrt{2}\sin m_n z, \quad \text{and} \quad \varpi = \sum_{n=1}^{\infty} \varpi_n(x, y, t)\sqrt{2}\cos m_n z, \tag{3.2a,b}$$

where the vertical wavenumber is

$$m_n \stackrel{\text{def}}{=} n\pi/d. \tag{3.3}$$

The modal amplitudes in (3.2) are given by

$$(w_n, \varpi_n) = \frac{1}{d}\int_{-d}^{0} (w, \varpi)\sqrt{2}(\sin m_n z, \cos m_n z)\,\mathrm{d}z. \tag{3.4}$$

Projecting the IW equation (2.22) onto the sine modes we obtain

$$[\partial_t^2(\partial_x^2 + \partial_y^2 - m_n^2) + N^2(\partial_x^2 + \partial_y^2)]w_n = \frac{\sqrt{2}m_n}{d}\partial_t^2\partial_x \mathrm{e}^{\delta t} M. \tag{3.5}$$

The forcing on the right-hand side of (3.5) comes from handling the $z$-derivatives in (2.22) with integration by parts.

Moving with the SW group, we look for a solution of (3.5) of the form $\mathrm{e}^{\delta t} w_n(\tilde{x}, y)$ where $\tilde{x}$ is the group coordinate defined in (2.12). Using the Fourier transform

$$\hat{w}_n(q, s) \stackrel{\text{def}}{=} \iint \mathrm{e}^{-\mathrm{i}(q\tilde{x}+sy)} w_n(\tilde{x}, y)\,\mathrm{d}\tilde{x}\,\mathrm{d}y, \tag{3.6}$$

the solution of (3.5) is

$$\hat{w}_n = -\frac{\sqrt{2}m_n}{d}\frac{\mathrm{i}q(q+\mathrm{i}\eta)^2\hat{M}(q, s)}{(q+\mathrm{i}\eta)^2(q^2+s^2+m_n^2) - q_{max}^2(q^2+s^2)}, \tag{3.7}$$

where

$$q_{max} \stackrel{\text{def}}{=} 2N/c, \quad \text{and} \quad \eta \stackrel{\text{def}}{=} 2\delta/c. \tag{3.8a,b}$$

| Parameter | Typical forcing | Extreme forcing |
|---|---|---|
| Wavenumber $k$ | $2\pi/(100\ \text{m})$ | $2\pi/(625\ \text{m})$ |
| Frequency $\sqrt{gk}$ | $2\pi/(8\ \text{s})$ | $2\pi/(20\ \text{s})$ |
| Phase speed $c=\sqrt{g/k}$, | $12.5\ \text{m s}^{-1}$ | $31\ \text{m s}^{-1}$ |
| Wave amplitude $a_{max}$ | 1 m | 4 m |
| Number of waves per group $n_{SW}$ | 5 | 5 |
| Group length $\ell_x=\pi n_{SW}/k$ | 250 m | 1.56 km |
| Group width $\ell_y$ | $3\ell_x=750$ m | $3\ell_x=4.69$ km |
| Depth $d$ | 2000 m | 2000 m |
| Depth-averaged buoyancy frequency $N$ | $2\pi/(2000\ \text{s})$ | $2\pi/(1333\ \text{s})$ |
| $q_{max}=2N/c$ | $2\pi/(12.5\ \text{km})$ | $2\pi/(20.8\ \text{km})$ |
| (SW group speed)/(IW phase speed) $m_{1*}=c\pi/2Nd$ | 3.125 | 5.2 |
| SW slope $\epsilon=a_{max}k$ | 0.0625 | 0.064 |
| Scale separation $\mu=(k\ell_x)^{-1}$ | 0.06 | 0.06 |

TABLE 1. Numerical values characteristic of swell and stratification; $g=9.81\ \text{m s}^{-2}$ and $\rho_0=1000\ \text{kg m}^{-3}$. Here we have picked parameters for short period, 1 m amplitude swell as a typical example, and long period 4 m amplitude swell as an example of extreme forcing. The depth-averaged stratification, $N$, is consistent with the phase speed of the first baroclinic mode for a depth $d=2000$ m. Figure 5 of Chelton *et al.* (1998) shows that the average phase speed of the first baroclinic mode varies with latitude between approximately $1.5\ \text{m s}^{-1}$–$3\ \text{m s}^{-1}$. The surface group length, $\ell_x$, is based on the assumption that a group is comprised of $n_{SW}$ consecutive waves that are at least half as high as the tallest in the group. While observations of wave group statistics in the North Sea (Battjes & Van Vledder 1984, figure 3*b*) and in coastal regions (Elgar, Guza & Seymour 1984) show that groups of one or two waves are far more likely, five wave groups are possible.

Projecting the pressure equation (2.23) onto the sine basis functions and then Fourier transforming, one finds that the modal amplitudes of the pressure field in (3.2) are

$$\hat{\varpi}_n = \frac{\mathrm{i}c}{2m_n}\frac{q_{max}^2-(q+\mathrm{i}\eta)^2}{(q+\mathrm{i}\eta)}\hat{w}_n. \tag{3.9}$$

The inverse Fourier transform of (3.7)

$$w_n = \iint_{-\infty}^{\infty}\hat{w}_n\mathrm{e}^{\mathrm{i}(q\tilde{x}+sy)}\frac{\mathrm{d}q\,\mathrm{d}s}{(2\pi)^2}, \tag{3.10}$$

$$= \iint_{(q,s)>0}\cos(sy)\mathrm{Re}[\hat{w}_n\mathrm{e}^{\mathrm{i}q\tilde{x}}]\,\mathrm{d}q\,\mathrm{d}s. \tag{3.11}$$

In passing from (3.10) to (3.11) we have exploited the symmetries $\hat{w}_n(q,s)=\hat{w}_n(q,-s)$ and $\hat{w}_n(q,s)=\hat{w}_n^{\star}(-q,s)$, where $^{\star}$ indicates the complex conjugate, to write the inverse Fourier transform as an integral over the first quarter of the wavenumber plane. Here we have assumed that $\hat{M}$ has these same symmetries.

The vertical velocity is obtained by numerical integration of (3.11) and for illustration we use the typical SW and stratification parameters given in table 1, and choose $\delta=3.1\times10^{-5}\ \text{s}^{-1}$ for our slow growth parameter. The horizontal structure

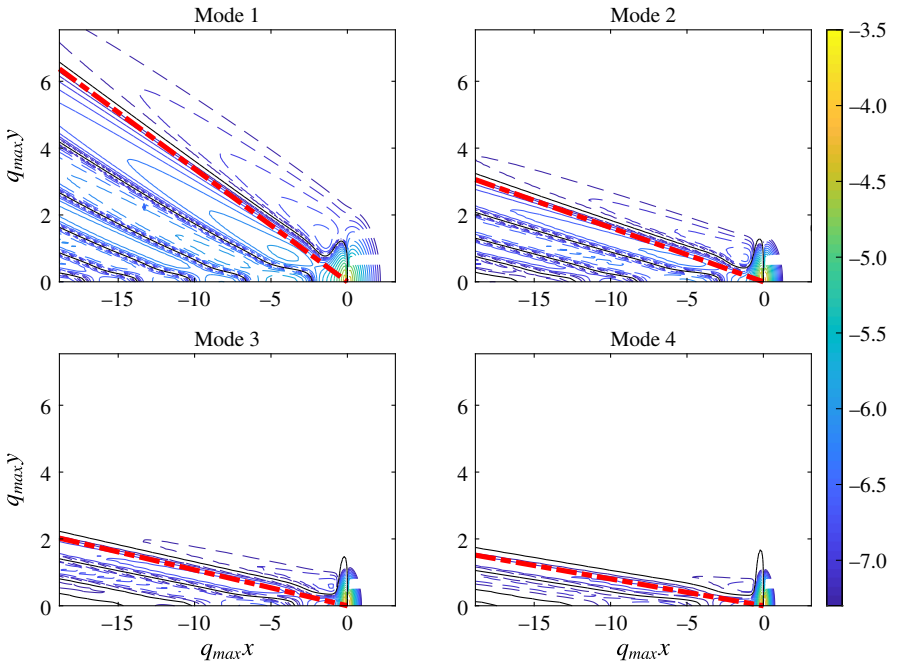


FIGURE 2. (Colour online) Common logarithm of $|w_n|$ for the first four modes. Dashed contours indicate negative vertical velocities. The SW group is centred at the origin. The SW and stratification parameters are given for the typical case in table 1. The thin black line is the contour where the vertical velocity vanishes. The red dash-dot line is the theoretical prediction for maximum wake angle given by (3.18).

of the first four vertical modes is shown in figure 2. Each mode shows a wake of IWs trailing behind the SW group, which is centred at the origin. Figure 3 shows the full vertical velocity for IWs radiated from an SW group passing over a uniformly stratified ocean. Figure 3 shows a strong Eulerian return flow in the forcing region with weaker vertical velocities associated with IWs trailing behind the forcing region. The solution is dominated by the first vertical mode.

### 3.2. *The singular curves*

Returning to (3.7), we see the problem of zero divisors if we set $\eta = 0$. With small non-zero $\eta$ the solution is concentrated in wavenumber space on the 'singular curve' where the denominator of (3.7) is close to zero. These curves are shown in the first quadrant of the $(q, s)$-plane in figure 4 for a few values of stratification, depth, and SW group speed. The singular curves are defined by the zeros of the function

$$\gamma(q, s) \stackrel{\text{def}}{=} q - q_{max}\sqrt{\frac{q^2 + s^2}{q^2 + s^2 + m_n^2}}. \tag{3.12}$$

The structure of these curves depends on the crucial non-dimensional parameter

$$m_{n*} \stackrel{\text{def}}{=} \frac{m_n}{q_{max}} = \frac{cn\pi}{2Nd}, \tag{3.13}$$

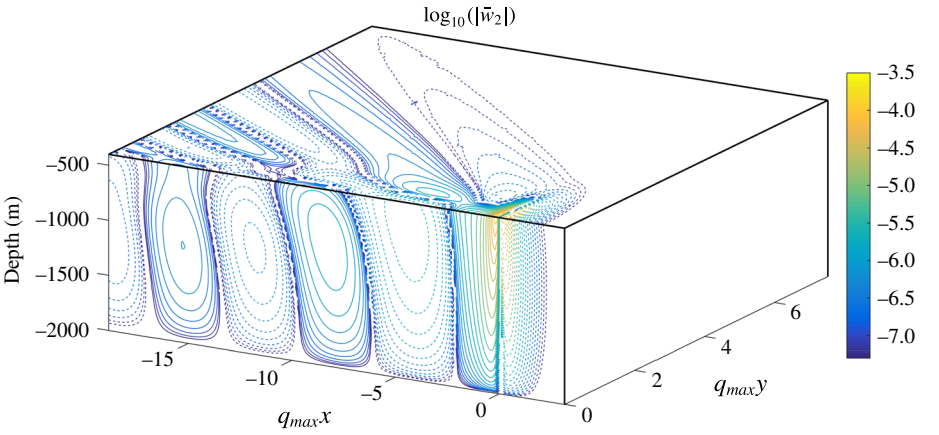


FIGURE 3. (Colour online) Common logarithm of $|\bar{w}_2|$. The SW group is centred at the origin and propagates in the positive $x$-direction. Dashed contours indicate negative vertical velocities. The typical SW and stratification parameters used are given in table 1. The solution shown is a numerical solution of (3.11) with $\delta = 3.1 \times 10^{-5}$ s$^{-1}$, with 200 vertical modes near the forcing region $[-0.1q_{max}x : 0.1q_{max}x]$ and 20 vertical modes in the rest of the domain.

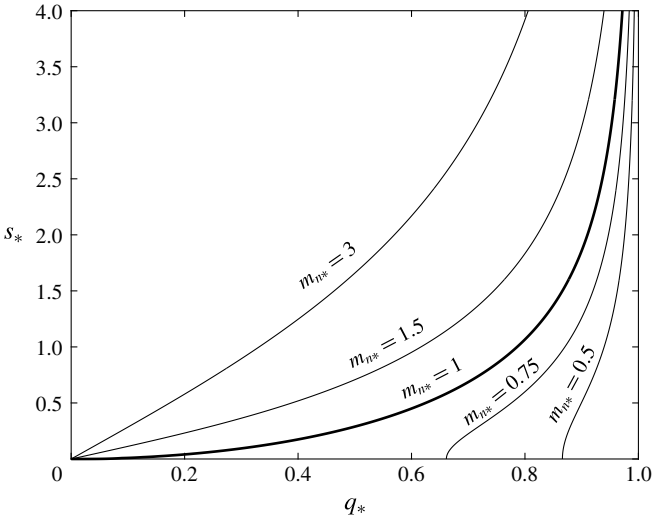


FIGURE 4. The singular curves defined by $\gamma(q, s) = 0$ in the first quadrant of the $(q_*, s_*)$-plane, where $q_* = q/q_{max}$, $s_* = s/q_{max}$, and $m_{n*} = m_n/q_{max}$. If $m_{n*} \geqslant 1$ the curve passes through the origin. The curve for $m_{n*} = 1$ is the thick black line.

which is the ratio of the SW group speed to the approximate IW phase speed of vertical mode $n$. Figure 4 shows that the case where $m_{n*} \leqslant 1$ is very different from the case $m_{n*} > 1$. In particular, in 2-D ($s = 0$), only cases with $m_{n*} < 1$ will radiate IWs, because only those singular curves intersect the $q$-axis. Further discussion of the 2-D problem is in § 5. The solution shown in figures 2 and 3 has $m_{n*} > 1$ for all vertical mode numbers $n$.

Using the definition of $q_{max}$, the condition $\gamma(q, s) = 0$ can be re-arranged as

$$\frac{c}{2} = \frac{N}{q}\sqrt{\frac{q^2+s^2}{q^2+s^2+m_n^2}}. \tag{3.14}$$

Recalling the IW dispersion relation for vertical mode $n$, namely $\omega^2 = N^2(q^2+s^2)/(q^2+s^2+m_n^2)$, we identify the right-hand side of (3.14) as the IW phase speed in the $x$-direction. Thus the singular curve (3.14) is the resonance condition that the $x$-phase speed of the IWs matches the group velocity $c/2$ of the SWs. Combining the IW dispersion relation and (3.14) we see that

$$\frac{\omega}{N} = \frac{q}{q_{max}}. \tag{3.15}$$

This relation shows there is an upper bound on the values of $q$ relevant for IW radiation: because $\omega < N$, wavenumbers with $q > q_{max}$ cannot radiate.

### 3.3. *The wake angle*

The stratification in the ocean is not sufficiently strong to support IWs that propagate at the SW group speed. However, if the radiated IWs propagate obliquely to the direction of SW group propagation then the point of intersection between the IW crest and the SW group can move with the SW group speed. To illustrate this, we will put ourselves in the reference frame moving with the SW group. Then the surrounding water is flowing backward at speed $c/2$. As shown in figure 5, the component of this backward flow that is parallel to the IW phase velocity must be equal in magnitude to the IW phase velocity. This geometric condition recovers the resonance condition

$$\frac{c}{2}\cos\chi_n = \frac{\omega}{\sqrt{q^2+s^2}}. \tag{3.16}$$

The wake angle $\theta_n$ is related to the direction of the phase velocity, $\chi_n$, by $\theta_n = \pi/2 - \chi_n$, so that $\cos\chi_n = \sin\theta_n$. Therefore the wake angle is given by

$$\sin\theta_n = \frac{2N}{c\sqrt{q^2+s^2+m_n^2}}, \tag{3.17}$$

where we have used the IW dispersion relation for $\omega(q, s)$. To find the widest possible wake angle $\theta_n$, we maximize the right-hand side of (3.17) over all wavenumbers by taking $q = s = 0$ to find

$$\max_{\forall(q,s)}(\sin\theta_n) = \frac{2N}{cm_n} = \frac{2Nd}{n\pi c} = \frac{1}{m_{n*}}. \tag{3.18}$$

The maximum wake angle is determined by the stratification, depth, and SW group speed. The first four modal constituents of vertical velocity $w_n(\tilde{x}, y)$ are shown in figure 2. The dashed red line at the angle determined by (3.18) is parallel to the zero contour (the solid, black line), indicating that wake angle predicted by (3.18) is accurate. (Recall in figure 2 that $m_{n*} > 1$ for all $n$.)

The maximum wake angle in (3.17) is undefined if $m_{n*} < 1$. This is the case if the stratification is strong so the fastest radiated IWs are moving at the SW group speed. Choosing even smaller values of $m_{n*}$ (larger $N$, larger $d$, or smaller $c/2$) does not change the wake angle beyond $\theta_n = \pi/2$.

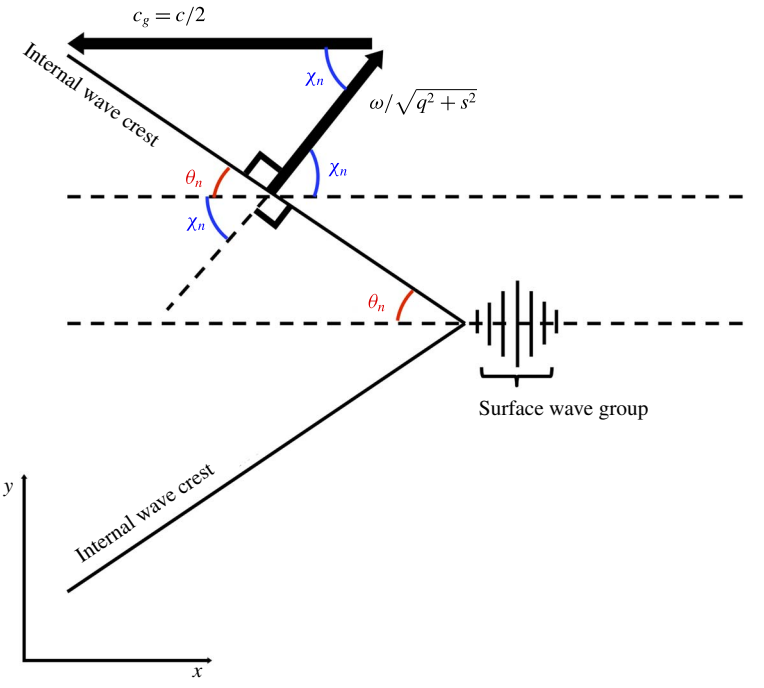


FIGURE 5. (Colour online) Schematic of the IW wake in the reference frame where the SW group is stationary. The surrounding water rushes backward (to the left) at the group speed $(c/2)$. The IW crest intersects the $x$-axis at an angle $\theta_n$, while the phase velocity of the IW, which is perpendicular to its crest, is at an angle of $\chi_n = \pi/2 - \theta_n$ to the $x$-axis. The condition in (3.16) is that the IW crest is stationary because the advance of phase normal to the crest is halted by the normal component, $(c/2)\cos\chi_n$, of the water velocity.

## 4. Energy flux into the IW field

The radiation of IWs from an SW group raises two questions: (i) Is the radiation of IWs a significant energy sink for the SWs? And (ii) is this radiation a significant source of energy for the IWs? In this section we compute the energy flux, and answer these questions with: (i) no and (ii) probably no, except maybe for strong stratification and large amplitude SWs.

### 4.1. *The radiation integral*

From (2.19)–(2.21) we obtain the second-order energy conservation equation

$$\partial_t \tfrac{1}{2}(|\boldsymbol{u}_2|^2 + N^{-2}\bar{b}_2^2) + \boldsymbol{\nabla}\cdot(\varpi\boldsymbol{u}_2) = 0. \tag{4.1}$$

Thus the vertical component of the energy flux at the surface is $\varpi\bar{w}_2|_0$; the total flux of energy out of the SW group and into the IW field in Watts is therefore $\rho_0 J$ where

$$J \overset{\text{def}}{=} \iint M_x \varpi \Big|_0 \,\mathrm{d}x\,\mathrm{d}y. \tag{4.2}$$

In (4.2) the surface boundary condition in (2.26) has been used for $\bar{w}_2|_0$. Using the modal expansion for $\varpi$ in (3.2) the right-hand side of (4.2) is

$$J = \sum_{n=1}^{\infty} \underbrace{\iint_{-\infty}^{\infty} M_x \varpi_n \Big|_0 \, \mathrm{d}x \, \mathrm{d}y}_{\stackrel{\text{def}}{=} J_n}, \tag{4.3}$$

where $J_n$ is the energy flux into vertical mode $n$.

With Parseval's theorem, we can express $J_n$ in terms of the Fourier transforms $\hat{M}$ and $\hat{\varpi}_n$ as

$$J_n = \iint_{-\infty}^{\infty} \mathrm{i}q\hat{M}\hat{\varpi}_n^{\star} \Big|_0 \frac{\mathrm{d}q \, \mathrm{d}s}{(2\pi)^2}. \tag{4.4}$$

The Fourier transform $\hat{\varpi}_n$ is given by (3.9) and thus the energy flux into vertical mode $n$ is $\rho_0 J_n$ where

$$J_n = \frac{c}{2}\frac{\sqrt{2}}{d} \iint_{-\infty}^{\infty} \frac{\mathrm{i}q^2[q_{max}^2 - (q-\mathrm{i}\eta)^2](q+\mathrm{i}\eta)|\hat{M}|^2}{(q-\mathrm{i}\eta)^2(q^2+s^2+m_n^2) - q_{max}^2(q^2+s^2)} \frac{\mathrm{d}q \, \mathrm{d}s}{(2\pi)^2}. \tag{4.5}$$

It is helpful to define

$$\cos^2\vartheta_n = \frac{m_n^2}{q^2+s^2+m_n^2}, \quad \sin^2\vartheta_n = \frac{q^2+s^2}{q^2+s^2+m_n^2}, \tag{4.6a,b}$$

so that the partial fraction decomposition of (4.5) can be written as

$$\begin{aligned} J_n = {} & \frac{c}{2}\frac{\sqrt{2}}{d} \iint_{-\infty}^{\infty} \frac{\mathrm{i}q^2|\hat{M}|^2}{q^2+s^2+m_n^2} \\ & \times \left[ q + \mathrm{i}\eta - \frac{1}{2}\frac{q_{max}^2\cos^2\vartheta_n}{q - \mathrm{i}\eta + q_{max}\sin\vartheta_n} - \frac{1}{2}\frac{q_{max}^2\cos^2\vartheta_n}{q - \mathrm{i}\eta - q_{max}\sin\vartheta_n} \right] \frac{\mathrm{d}q \, \mathrm{d}s}{(2\pi)^2}. \end{aligned} \tag{4.7}$$

We can drop the term $q+\mathrm{i}\eta$ in the square bracket above: the $q$ is an odd function that integrates to zero and the $\mathrm{i}\eta$ is a non-singular term that vanishes in the limit $\eta \to 0$. The remaining terms in the integral are even in both $q$ and $s$ and taking advantage of these symmetries we can restrict the integration to the first quadrant to obtain

$$J_n = -\frac{c}{2}\frac{4\pi q_{max}^2 m_n^2}{\sqrt{2}d} \iint_{(q,s)>0} \frac{q^2|\hat{M}|^2}{(q^2+s^2+m_n^2)^2} \frac{1}{\pi} \frac{\eta}{(q - q_{max}\sin\vartheta_n)^2 + \eta^2} \frac{\mathrm{d}q \, \mathrm{d}s}{(2\pi)^2}. \tag{4.8}$$

Taking the limit $\eta \to 0$ in (4.8) using the result in appendix B, we find that the double integral is concentrated on the singular curves given by the zeros of $\gamma(q,s)$ in (3.12), and shown in figure 4. Thus, after the limit $\eta \to 0$ the double integral in (4.8) is reduced to a single integral with respect to $q$:

$$J_n = -\frac{c}{2}\frac{1}{\sqrt{2}\pi d} \int_{q_{min}}^{q_{max}} q^2|\hat{M}(q, s_n(q))|^2 \sqrt{\frac{q_{max}^2 - q^2}{m_n^2 - q_{max}^2 + q^2}} \, \mathrm{d}q. \tag{4.9}$$

In the second argument of $\hat{M}$ in (4.9), the singular curves defined by $\gamma(s,q)=0$, with $\gamma(s,q)$ in (3.12), are parameterized by $q$ as $s=s_n(q)$, where

$$s_n(q) \overset{\text{def}}{=} q\sqrt{\frac{m_n^2-q_{max}^2+q^2}{q_{max}^2-q^2}}. \tag{4.10}$$

The upper limit of integration in (4.9) is $q_{max}=2N/c$ and the lower limit is

$$q_{min} \overset{\text{def}}{=} \begin{cases} 0, & \text{if } q_{max}\leqslant m_n; \\ \sqrt{q_{max}^2-m_n^2}, & \text{if } q_{max}\geqslant m_n. \end{cases} \tag{4.11}$$

The definition of $q_{min}$ above corresponds to the distinction between the curves in figure 4 corresponding to $m_{n*}\geqslant 1$, which pass through the origin, and those curves with $m_{n*}<1$ which cross the $q$ axis at $\sqrt{q_{max}^2-m_n^2}$. Both types of curves asymptote to $s=\infty$ as $q\to q_{max}$: this asymptote corresponds to the upper limit of integration in (4.9). In physical terms there is a 'cutoff' wavenumber $q_{max}$ because IWs have frequencies less than $N$: wavenumbers $q>q_{max}$ correspond the non-existent IWs with frequencies greater than $N$.

The 'radiation integral' on the right of (4.9) is our most general expression for the energy lost to mode-$n$ internal gravity waves from the SW group. We make approximations to (4.9) assuming realistic SW and stratification parameters in § 4.3.

### 4.2. *Energy transfer between a Gaussian SW group and the IW wake*

To make a simple estimate of the energy loss from surface gravity waves we adopt the Gaussian model from appendix A and use numerical values in table 1. Since energy in the SWs is partitioned equally between kinetic and potential, the energy density of an SW train is given by $gh_1^2$ (Phillips 1977). Then using $h_1$ in (2.10) and the Gaussian wave envelope in (A 1) the total energy of the packet is $\rho_0 E$, in Joules, where

$$E=\iint gh_1^2\,\mathrm{d}x\,\mathrm{d}y=\frac{\pi}{2}ga_{max}^2\ell_x\ell_y. \tag{4.12}$$

Next we non-dimensionalize (4.9) as before using $q_*=q/q_{max}$ and $m_{n*}=m_n/q_{max}$ and replace $|\hat{M}|^2$ by the Gaussian expression (A 3). Using $c^2k=g$, we find

$$J_n = -\frac{q_{max}^3}{2\sqrt{2}\pi cd}\left(\frac{\pi}{2}ga_{max}^2\ell_x\ell_y\right)^2 \times \underbrace{\int_{q_{min*}}^1 q_*^2\exp\left[-\frac{1}{2}(q_{max}\ell_x)^2q_*^2\left(1+\frac{m_{n*}^2-1+q_*^2}{1-q_*^2}\frac{\ell_y^2}{\ell_x^2}\right)\right]\sqrt{\frac{1-q_*^2}{m_{n*}^2-1+q_*^2}}\,\mathrm{d}q_*}_{\mathcal{J}_n(q_{max}\ell_x,\ell_y/\ell_x,m_{n*})}, \tag{4.13}$$

where

$$q_{min*}=\begin{cases}\sqrt{1-m_{n*}^2}, & \text{if } m_{n*}<1; \\ 0, & \text{if } m_{n*}\geqslant 1.\end{cases} \tag{4.14}$$

Using the values in table 1, $q_{min*}=0$.

Now we consider the slow time evolution of the SWs and assume that only the IW radiation affects the energy tendency:

$$E_t = \sum_{n=1}^{\infty} J_n, \tag{4.15}$$

$$= -\underbrace{\frac{q_{max}^3}{2\sqrt{2}\pi cd}\sum_{n=1}^{\infty}\mathcal{J}_n}_{\stackrel{\text{def}}{=}\alpha}\underbrace{\left(\frac{\pi}{2}ga_{max}^2\ell_x\ell_y\right)^2}_{E^2}. \tag{4.16}$$

In (4.16) we have expressed the energy flux in terms of the energy in the wave group, and the factor $\alpha$. We assume that $\alpha$ is constant as $E \propto a_{max}^2$ slowly decreases due to radiative damping. Then the solution of the differential equation (4.16) is

$$E = \frac{E_0}{1+\alpha E_0 t}, \tag{4.17}$$

where $E_0$ is the initial energy corresponding to the initial $a_{max}$. Therefore the half-life of a group of SWs is given by

$$t_{1/2} = \frac{1}{\alpha E_0} = \frac{c^4 d}{\sqrt{2}gN^3a_{max}^2\ell_x\ell_y\sum_{n=1}^{\infty}\mathcal{J}_n} = -\frac{E_0}{\sum_{n=1}^{\infty}J_n}, \tag{4.18}$$

where $a_{max}$ and $J_n$ above are evaluated at $t=0$. Equation (4.18) highlights that faster waves in a deeper ocean survive longer, while larger waves, larger wave groups and stronger stratification damp the wave group more quickly.

Computing the energy flux from SWs to IWs by numerical evaluation of the integral for $J_n$ in (4.13) we find that the radiated energy into the first 5 vertical modes is approximately 0.2 W for typical forcing and approximately 100 W for extreme forcing in table 1. In the extreme forcing case, it would take over 100 000 days (and much more for the typical case) for the SWs to lose half their energy. In this time the wave group would have travelled more than 1000 times around the Earth. We can safely say that this is a small loss of energy from the SWs.

Might this small energy flux be a significant energy source for the IW field? The ocean IW spectrum has two peaks: the near-inertial spectral peak and a secondary peak at frequencies close to the buoyancy frequency $N$ (Pinkel 1975). As Olbers & Eden (2016) note, the energy flux from SWs to IWs is small compared to the energy flux from the wind into near-inertial waves. However, figure 6 (which is discussed in more detail in § 4.3) shows that the majority of the energy radiated from SWs goes into near-$N$ IWs. The amplitude of the near-$N$ spectral peak is much smaller than that of the near-inertial spectral peak, so the energy flux estimated above may be significant for near-$N$ IWs while also negligible compared to the energy flux due to wind forcing. From figure 6 of Pinkel (1975) we estimate this peak in isotherm displacement squared $\zeta'^2$ to be 0.5 m$^2$ (cycles per hour)$^{-1}$ in amplitude, and 2 cycles per hour wide. Then we can estimate the near-$N$ IW energy density as $\rho N_{pyc}^2\zeta'^2 d$, where $N_{pyc} = 2\pi/(900\text{ s})$ is a typical stratification in the pycnocline. The power density of IW radiation from SW forcing is $\rho_0\sum_{n=1}^{5}J_n/\ell_x\ell_y$. Then a time scale of forcing, $\tau$, can be obtained by dividing observations of energy density by the power density to

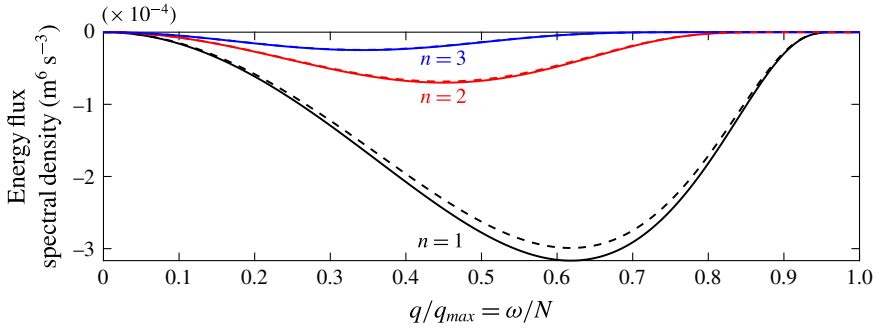


FIGURE 6. (Colour online) The energy flux spectral density for the typical SW and stratification parameters in table 1. The solid lines show the exact integrand in (4.13), and the dashed lines show the approximation in (4.20) for the first three vertical modes as a function of normalized horizontal wavenumber, $q/q_{max}$, which is equivalent to the IW frequency, $\omega$, normalized by the buoyancy frequency $N$.

find $\tau \approx 500$ days in the typical case and $\tau \approx 1$ day in the extreme case. This implies that one day of extreme forcing by SW groups with these parameters would produce the measured amount of near-$N$ IW energy. Therefore, this mechanism is likely not a source of near-$N$ IWs under typical SW forcing, but may be significant during extreme forcing.

### 4.3. *The limit of weak stratification and fast SWs*

Figure 2 of Chelton *et al.* (1998), shows a global map of the fastest possible IW phase speed based on observations of the vertically integrated stratification, $\int_{-d}^{0} N(z)\,\mathrm{d}z$ and assuming hydrostatic IWs. The hydrostatic approximation results in an overestimate of the IW phase speed, so these estimates are used as an upper bound. The map shows that IW phase speeds never exceed 3.2 m s$^{-1}$, and generally range from 1 to 3 m s$^{-1}$ for the first baroclinic mode. If we consider swell with periods of 8 or larger, then

$$m_{n*} = \frac{cn\pi}{2Nd} \gtrsim 2. \tag{4.19}$$

In other words, for SWs with periods of 8 or longer, the SW group speed is always significantly greater than the IW phase speed. In this sense the ocean stratification is weak, IWs are slow, and the SWs are fast. Thus the relevant case in (4.14) is $m_{n*} > 1$ and $q_{min*} = 0$. The other case, $m_{n*} < 1$ and $q_{min*} = \sqrt{1 - m_{n*}^2}$, is not relevant for Earth's oceans.

Equation (4.13) is opaque: the dependence of $J_n$ on key parameters is buried inside a difficult integral. We will exploit the weak stratification and fast SWs to approximate (4.13), and reveal the dependence of $J_n$ on the stratification and SW parameters. After systematic simplification of the integrand in (4.13) assuming $m_{n*}^2 \gg 1$, and $\ell_y > \ell_x$, we have

$$J_n \approx -\frac{1}{n}\frac{\sqrt{2}}{c}(Na_{max})^4 (k\ell_x\ell_y)^2 \underbrace{\int_0^1 q_*^2 \exp\left[-\frac{q_*^2}{1-q_*^2}\frac{(m_n\ell_y)^2}{2}\right]\sqrt{1-q_*^2}\,\mathrm{d}q_*}_{\mathcal{K}_n(m_n\ell_y)}. \tag{4.20}$$

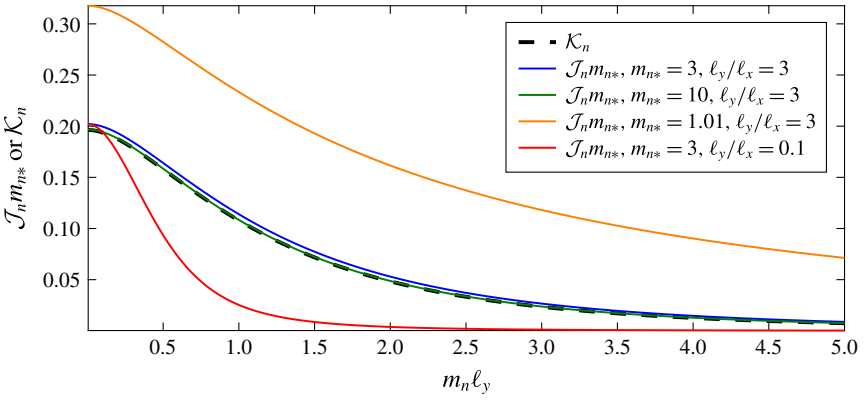


FIGURE 7. (Colour online) The approximate dimensionless integral $\mathcal{K}_n$ (dashed) compared with exact solutions $\mathcal{J}_n m_{n*}$ (solid) over a range of the control parameters $m_n \ell_y$. The approximation agrees well in two cases where the assumptions ($m_{n*}^2 \gg 1$ and $\ell_y > \ell_x$) are met (blue and green). The approximation is very poor when the assumptions are not met (orange and red).

Above, $\mathcal{K}_n$ is an $m_{n*}^2 \gg 1$ approximation to the integral $m_{n*}\mathcal{J}_n$ in (4.13). Using the typical wave and stratification parameters assumed in table 1, the approximate integrand in (4.20), is very close to the exact integrand in (4.13): see figure 6. Note that while the exact $\mathcal{J}_n$ in (4.13) depends on three parameters, the approximation $\mathcal{K}_n$ in (4.20) contains only the single parameter $m_n \ell_y$, which is equal to the product of the three parameters in $\mathcal{J}_n$. Therefore

$$J \approx -\frac{\sqrt{2}}{c}(Na_{max})^4 (k\ell_x \ell_y)^2 \sum_{n=1}^{\infty} \frac{1}{n} \mathcal{K}_n(m_n \ell_y), \tag{4.21}$$

provided that $m_{n*}^2 \gg 1$ and $\ell_y/\ell_x > 1$.

Figure 7 shows the dependence of the integral $\mathcal{K}_n$ on the control parameter $m_n \ell_y$. The dashed line is $\mathcal{K}_n$, and the solid lines are exact solutions $\mathcal{J}_n m_{n*}$ from (4.13). The approximation agrees well with the two exact solutions with parameters that satisfy the assumptions $m_{n*}^2 \gg 1$ and $\ell_y > \ell_x$, and very poorly with cases that do not satisfy these assumptions.

We see from (4.21) and from figure 7 that the energy flux decreases quickly with increasing $n$. This is also clear in figure 6. Therefore, neglecting all but the first mode, the energy flux becomes

$$J \approx J_1 \approx -\frac{32\sqrt{2}\pi^5}{g^3} \frac{(Na_{max})^4}{T^5} (\ell_x \ell_y)^2 \mathcal{K}_1(m_1 \ell_y), \tag{4.22}$$

where we have replaced the wavenumber $k$ and phase speed $c$ with an expression including $g$ and the SW period $T$ using the deep water dispersion relation. Using a spectrum of waves, Olbers & Eden (2016) recover the same dependence on stratification, SW period and nearly the same dependence on SW amplitude. (Olbers & Eden (2016) present their results in terms of the wind speed. The energy flux in their equation (35) varies as wind speed to the seventh power, and they assume a parametrization in which the wave amplitude is proportional to the wind speed

squared. Not included in their paper is a non-dimensional form of the radiative transfer which recovers the $T^{-5}$ dependence as well, Dirk Olbers 2017, personal communication.) From (4.22) it is clear that the SW amplitude, stratification, and wave period are the strongest controlling parameters. Thus even small changes in $T$, $a_{max}$, or $N$ can drastically change the rate of energy flux from SWs to IWs.

### 4.4. *Long-crested SWs*

An even simpler approximation is obtained if $m_n\ell_y$ is large: as $m_n\ell_y \to \infty$ we have $\mathcal{K}_n \sim 2^{-1/2}\pi^{-5/2}(d/n\ell_y)^3$. In this case, with long-crested wave groups, (4.21) simplifies to

$$J \approx -\frac{d^3}{\pi^{5/2}c\ell_y}(Na_{max})^4(k\ell_x)^2 \underbrace{\sum_{n=1}^{\infty}\frac{1}{n^3}}_{\approx 1.2}, \tag{4.23}$$

provided $m_{n*}^2 \gg 1$, $\ell_y > \ell_x$ and $m_n\ell_y \gg 1$. Note that (4.23) is a very poor approximation for our assumed typical parameters ($m_n\ell_y \approx 1$), but the range of validity of this approximation is not far from the assumed parameter values. Nevertheless, the $m_n\ell_y \gg 1$ approximation is valid for high vertical modes $n \gg 1$. This approximation highlights the weak dependence of the energy flux on the width of the group $\ell_y$ and the strong dependence on the depth $d$.

## 5. The two-dimensional case

The 2-D problem, with no dependence on $y$, is significantly simpler than the 3-D problem discussed in the previous sections. In two dimensions, the streamfunction–vorticity formulation provides a compact solution of the second-order wave-averaged equations of motion. Moreover, strictly in two dimensions, Lighthill (1978) in § 3.9 and Lamb (1932) in § 249, provide a resolution of the radiation condition that avoids the technicalities of zero divisors and the $\eta \to 0$ limit in appendix B. Furthermore, although the 2-D case can be recovered as a special case of our previous 3-D results by taking $\ell_y \to \infty$, the limit requires evaluation of some singular integrals and is difficult to extract. Thus in this section we solve the 2-D problem from the beginning and then show how these result can be recovered from the 3-D solution as a special case. This alternative derivation provides a significant check on the 3-D solution.

### 5.1. *Solution of the 2-D problem*

With no $y$ dependence the IW equation for vertical velocity (2.22) is

$$[\partial_t^2(\partial_x^2 + \partial_z^2) + N^2\partial_x^2]\bar{w}_2 = 0. \tag{5.1}$$

It will be convenient to introduce the streamfunction $\psi$, such that $\bar{w}_2 = \psi_x$, and $\bar{u}_2 = -\psi_z$. Replacing $\bar{w}_2$ by $\psi$ and moving into the wave group frame, we have

$$(\partial_{\tilde{x}}^2 + \partial_z^2 + q_{max}^2)\psi = 0, \tag{5.2}$$

where recall $q_{max} = 2N/c$. The surface boundary condition in (2.26) is equivalent to $\psi(\tilde{x}, 0) = M(\tilde{x})$. Then projecting (5.2) onto the sine modes defined in (3.4), we find that the evolution equation for amplitude of mode $n$ is

$$[\partial_{\tilde{x}}^2 + \underbrace{q_{max}^2(1 - m_{n*}^2)}_{\stackrel{\text{def}}{=} q_{min}^2}]\psi_n = \frac{\sqrt{2}m_n}{d}M^{1D}, \tag{5.3}$$

with $m_{n^*} = m_n/q_{max}$ and $M^{1D}(\tilde{x})$ is the one-dimensional Gaussian envelope in (A 4). In this 2-D case we do not need to consider a slowly growing wave group in order to implement the radiation condition i.e. $M^{1D}$ on the right of (5.3) is not growing.

Notice that (5.3) further elucidates the importance of the critical parameter $m_{n*}$. In two dimensions, when $m_{n*} < 1$, solutions to (5.3) are propagating waves. This case corresponds to the singular curves that intersect the $q$-axis at $q = q_{min}$ in figure 4. On the other hand, if $m_{n*} > 1$ then solutions of (5.3) are evanescent i.e. exponentially trapped around the forcing $M^{1D}$. This case corresponds to a return flow comprised of the evanescent modes similar to the unstratified case depicted in figure 1(*a*). Because $m_{n*} \propto n$, in two dimensions there is a vertical mode number $n_{rad}$ above which $m_{n*} > 1$ i.e. modes with $n > n_{rad}$ are evanescent and contribute to the return flow and not to radiation of IWs. If the stratification is weak (and the stratification of the ocean is weak in this sense) then $n_{rad} < 1$ and all vertical modes are evanescent. (Whereas in three dimensions all modes are radiate.)

To solve (5.3) we employ Green's functions. First consider the radiating modes with $q_{min}^2 > 0$. The Green's function $G(\tilde{x})$ is defined by

$$(\partial_{\tilde{x}}^2 + q_{min}^2) G_n = \delta(\tilde{x}), \tag{5.4}$$

with solution

$$G_n(\tilde{x}) = -\frac{\sin q_{min}\tilde{x}}{q_{min}} H(-\tilde{x}), \tag{5.5}$$

where $H(-\tilde{x})$ is Heaviside step function. The factor $H(-\tilde{x})$ ensures that the solution in (5.5) satisfies the radiation condition: radiated IWs trail behind ($\tilde{x} < 0$) the SW forcing. This choice of Heaviside function is analogous to choosing the sign of $\delta$ in (3.1). Using this Green's function the streamfunction for radiating modes with $1 \leqslant n \leqslant n_{rad}$ is

$$\psi_n(\tilde{x}) = -\frac{\sqrt{2} m_n}{q_{min} d} \int_{\tilde{x}}^{\infty} M^{1D}(x') \sin[q_{min}(\tilde{x} - x')] \, \mathrm{d}x'. \tag{5.6}$$

Turning to the evanescent modes with $q_{min}^2 < 0$, we introduce $\beta_n^2 = -q_{min}^2 > 0$. Then the relevant solution of (5.4) is

$$G_n(\tilde{x}) = -\frac{\mathrm{e}^{-\beta_n|\tilde{x}|}}{2\beta_n}, \tag{5.7}$$

and the streamfunction for evanescent modes with $n > n_{rad}$ is

$$\psi_n(\tilde{x}) = -\frac{\sqrt{2} m_n}{2\beta_n d} \int_{-\infty}^{\infty} M^{1D}(x') \mathrm{e}^{-\beta_n|\tilde{x} - x'|} \, \mathrm{d}x'. \tag{5.8}$$

To compute the energy flux, we first consider the solutions in (5.6) and (5.8) far in the wake of the SW packet i.e. as $\tilde{x} \to -\infty$. In the wake, the evanescent modal amplitudes in (5.8) have decayed to zero and one is left with only the radiating modes with $n \leqslant n_{rad}$. Moreover, the integral in (5.6) is simplified by taking the lower limit to $-\infty$ so that

$$\psi_n = -\frac{\sqrt{2} m_n}{q_{min} d} \mathrm{Im}[\hat{M}^{1D}(q_{min}) \mathrm{e}^{\mathrm{i} q_{min}\tilde{x}}], \tag{5.9}$$

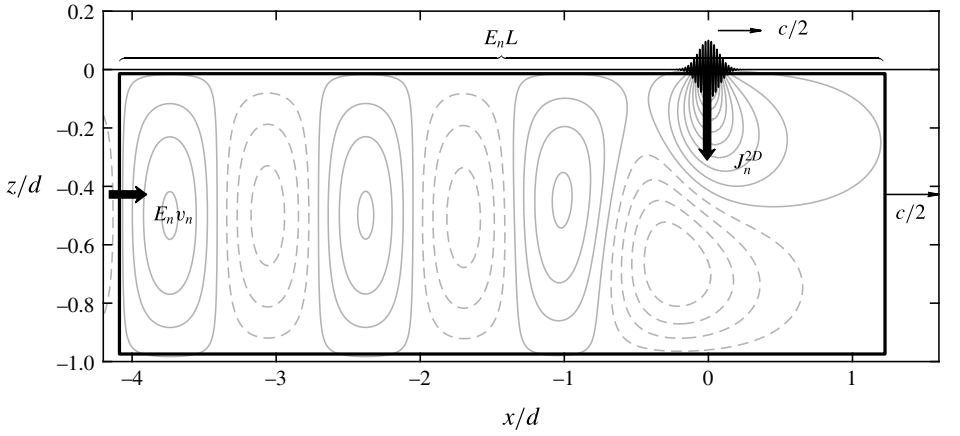


FIGURE 8. The flow as in figure 1(*b*) is used here to illustrate the energy flux calculation (5.13)–(5.14). The thick rectangle defines a 'control box'. The left edge of this box (at $x/d \approx -4$) is fixed far from the SW group. The right edge of the box moves with the SW group at speed $c/2$. Energy from previously generated IWs is carried into the box through the left edge at a rate $E_n\upsilon_n$. Energy also enters the box via a downward flux from the SW group.

where $\hat{M}^{1D}(q_{min})$ is the Fourier transform of $M^{1D}(\tilde{x})$ evaluated at the wavenumber $q_{min}$ and Im is the imaginary part. Thus in the wake

$$\langle \psi_n^2 \rangle = \frac{1}{2}\left(\frac{\sqrt{2}m_n}{q_{min}d}\right)^2 |\hat{M}^{1D}(q_{min})|^2, \tag{5.10}$$

where $\langle\ \rangle$ denotes a phase average of the IW i.e. an integral in $\tilde{x}$ over one wavelength $2\pi/q_{min}$. The potential energy density is $b^2/N^2 = q_{max}^2\psi^2$, so the IW energy density in the wake of the SW packet is therefore

$$\frac{1}{2}\int_{-d}^{0} \langle \psi_{\tilde{x}}^2 + \psi_z^2 + q_{max}^2\psi^2 \rangle \, \mathrm{d}z = \sum_{n=1}^{n_{rad}} E_n, \tag{5.11}$$

where the energy density of mode $n$ is

$$E_n = \underbrace{\frac{1}{2}\left(\frac{\sqrt{2}m_n}{q_{min}d}\right)^2 |\hat{M}^{1D}(q_{min})|^2}_{\langle\psi_n^2\rangle} q_{max}^2 d. \tag{5.12}$$

We can relate the energy density of the $n$th mode to the radiative flux using an argument given by Lamb (1932) in the context of SW resistance to a moving body. Figure 8 shows the wake of IWs behind an SW group as in figure 1(*b*). To compute the energy flux we first consider the total energy inside a box with left edge fixed far from the SW forcing region, and with the right edge of the box just in front of, and moving along with, the SW group at speed $c/2$. The energy in this 'control box' for the $n$th mode is $E_nL(t)$, where $L(t)$ is the length of the box. Then the energy flux

into this box can be written as a sum of the energy flux from the SW forcing $J_n^{2D}$, and the energy flux from IWs as they propagate through the left side of the box with their group speed $\upsilon_n$. Thus the energy conservation equation for the control box is

$$\partial_t(E_n L) = J_n^{2D} + E_n \upsilon_n. \tag{5.13}$$

Now $L = ct/2$, where $t$ is the time since the SW group entered the box by passing through the left edge and so from (5.13) we obtain Lamb's result

$$J_n^{2D} = E_n(\tfrac{1}{2}c - \upsilon_n). \tag{5.14}$$

The IW group velocity $\upsilon_n$ in (5.14) can be expressed in terms of the IW phase speed for a radiating wave, $c/2$, and the critical parameter $m_{n*}$ as

$$\upsilon_n = \frac{c}{2} m_{n*}^2. \tag{5.15}$$

Using expression (5.15) for the group velocity $\upsilon_n$, the radiative flux for the $n$th vertical mode given by (5.14) is

$$J_n^{2D} = \frac{c m_n^2}{2d} |\hat{M}^{1D}(q_{min})|^2. \tag{5.16}$$

In the illustrative case of a Gaussian envelope in (A 4) and (A 5), the radiation flux in (5.16) is

$$J_n^{2D} = -\frac{m_n^2}{2cd}\left(\frac{\sqrt{\pi}}{2} g a_{max}^2 \ell_x\right)^2 \mathrm{e}^{-(q_{min}\ell_x)^2/2}. \tag{5.17}$$

### 5.2. *The $\ell_y \to \infty$ limit of the 3-D solution illustrated with a Gaussian wave packet*

Throughout this section, we assume that $m_{n*} < 1$ so that $q_{min}$ in (5.3) is real. This condition is necessary for the radiation of IW energy: with $s = 0$ the resonance condition for vertical mode $n$ is that $c/2$ is equal to $N/\sqrt{q^2 + m_n^2}$, or equivalently that $q$ is equal to $q_{min}$ in (4.9) and figure 4. The results of Chelton *et al.* (1998) indicate that throughout Earth's ocean the SW group speed, $c/2$, for swell is likely greater than the IW phase speed $N/m_n$ for all $n$. In which case $q_{min}$ in (5.3) is imaginary and there is no radiation.

Nonetheless, as a consistency check on the previous 3-D calculations, it is interesting to suppose that $q_{min}$ is real and show that the 2-D result in (5.17) is recovered by taking the limit $\ell_y \to \infty$ in the 3-D radiation integral (4.9). The $\ell_y \to \infty$ limit is tricky e.g. as $\ell_y \to \infty$, $\hat{M}(q, s) \propto \delta(s)$ and a straightforward calculation using (4.9) requires consideration of $|\hat{M}|^2 \propto \delta[s_n(q)]^2$. The argument of the squared $\delta$-function, $s_n(q)$, is zero at $q = q_{min}$. But at this same point the big square root in (4.9) has an integrable singularity.

To avoid involvement with these duelling singularities, we first insert $|M|^2$ in (A 3) into (4.9) and then consider $\ell_y \to \infty$:

$$J_n = -\frac{1}{2\pi cd}\left(\frac{\pi}{2} g a_{max}^2 \ell_x\right)^2 \sqrt{\pi}\ell_y \times \int_{q_{min}}^{q_{max}} q^2 \mathrm{e}^{-(q\ell_x)^2/2} \underbrace{\sqrt{\frac{q_{max}^2 - q^2}{m_n^2 - q_{max}^2 + q^2}}}_{q/s_n(q)} \underbrace{\lim_{\ell_y\to\infty} \frac{\ell_y}{\sqrt{2}} \frac{1}{\sqrt{\pi}} \mathrm{e}^{-(s_n(q)\ell_y)^2/2}}_{\to \delta[s_n(q)]} \mathrm{d}q. \tag{5.18}$$

The factor $\ell_y$ left outside the integral in (5.18) is expected on physical grounds: the radiation should be linearly proportional to the length in $y$ of the SW packet.

Now recall that $s_n(q)$ is defined in (4.10), and observe that $s_n(q_{min}) = 0$. We can now simplify the integrand in (5.18) using a standard results for $\delta$-functions:

$$\frac{q}{s_n(q)}\delta[s_n(q)] = \frac{q}{s_n(q)}\frac{\delta(q-q_{min})}{\mathrm{d}s_n/\mathrm{d}q}, \tag{5.19}$$

$$= \frac{m_n^2}{q_{min}^2}\delta(q-q_{min}). \tag{5.20}$$

Evaluating (5.18) with the $\delta$-function in (5.20) we obtain

$$J_n = \sqrt{\pi}\ell_y J_n^{2D}, \tag{5.21}$$

where $J_n^{2D}$ is given by (5.17) and $\sqrt{\pi}\ell_y$ is the effective length in $y$ of the SW packet.

## 6. Discussion

As SW groups pass over the ocean, water is pumped downward in front of the group and lifted in the rear of the group, inducing a deep return flow. This Stokes pumping is a result of stronger Stokes drift in the centre of the group than at the edges, producing a divergence in the mass flux. Without stratification, this produces the deep return flow with momentum equal in magnitude but opposite in direction to the momentum of the shallow Stokes drift. As these wave groups pass over a uniformly stratified ocean, the isopycnals are set into motion by the return flow, generating a trailing wake of internal gravity waves.

The pattern of radiated IWs is stationary in the frame of reference of the SW group, just as ship wake waves are stationary relative to the ship. Because the stratification in the ocean is relatively weak, there are rarely if ever IWs that propagate with phase speeds as fast as the group speed of swell ($\gtrsim 6$ m s$^{-1}$). Thus radiated IWs must propagate obliquely to the direction of SW propagation so that the IW phase speed in the SW direction is much faster than the IW phase speed normal to the wave crests.

The wake angle can be predicted as a function of the vertical mode number, stratification, SW group speed, and ocean depth. The full wake solution shows a wake at nearly the angle appropriate for a mode one wave. This is consistent with the fact that most of the radiated energy is put into mode one IWs at frequencies near the buoyancy frequency.

Using typical parameters for SWs, and ocean stratification, we find that the total energy transfer from SWs to IWs is insignificant. However, when the SWs have very large amplitude, and when the stratification is strong, the radiation of IWs may be a significant source for near-$N$ IWs. Pinkel (1975) observed a near-$N$ spectral peak of IW energy. The energy content of this peak divided by the energy flux from SWs to IWs, under extreme forcing, gives a time scale of approximately one day. This implies that this forcing mechanism acting over a day would generate IWs at near-$N$ frequencies with the observed amount of energy. Therefore, although the very large amplitude swell assumed in this estimate is not present everywhere all of the time, it suggests that SW forcing may at least contribute to the observed near-$N$ peak in IW energy.

**Acknowledgements**

This work was supported by National Science Foundation award OCE-1357047. We thank R. Pinkel for helpful discussions. We also thank D. Olbers, P. Smit and an anonymous reviewer for suggestions that improved this work.

## Appendix A. A Gaussian envelope

For illustrative purposes we use the Gaussian envelope function

$$a = a_{max} \exp\left(-\frac{\tilde{x}^2}{2\ell_x^2} - \frac{y^2}{2\ell_y^2}\right), \tag{A 1}$$

where $\tilde{x}$ is the group coordinate in (2.12). With the envelope in (A 1) the wave momentum (2.15) is

$$M(\tilde{x}, y) = \frac{1}{2} c k a_{max}^2 \exp\left(-\frac{\tilde{x}^2}{\ell_x^2} - \frac{y^2}{\ell_y^2}\right). \tag{A 2}$$

Using the Fourier transform defined in (3.6) we have

$$\hat{M}(q, s) = \frac{1}{2} c k a_{max}^2 \ell_x \ell_y \pi \exp\left[-\left(\frac{q\ell_x}{2}\right)^2 - \left(\frac{s\ell_y}{2}\right)^2\right]. \tag{A 3}$$

In the radiation integral for $J_n$ in (4.9) we have $|\hat{M}|^2$.

In § 5 we consider the 2-D problem with a Gaussian envelope

$$M^{1D}(\tilde{x}) = \tfrac{1}{2} c k a_{max}^2 \mathrm{e}^{-\tilde{x}^2/\ell_x^2}, \tag{A 4}$$

with Fourier transform

$$\hat{M}^{1D}(q) = \tfrac{1}{2} c k a_{max}^2 \sqrt{\pi} \ell_x \mathrm{e}^{-(\ell_x q/2)^2}. \tag{A 5}$$

## Appendix B. A $\delta$-function limit

The radiation integral in (4.8) has the form

$$I \stackrel{\text{def}}{=} \lim_{\eta \to 0} \iint F(q, s) \frac{1}{\pi} \frac{\eta}{\gamma(q, s)^2 + \eta^2} \, \mathrm{d}q \, \mathrm{d}s, \tag{B 1}$$

where the function $\gamma(q, s)$ defined in (3.12) is zero on the 'singular curve' $\mathcal{C}$. In the limit $\eta \to 0$, the double integral in (B 1) can be reduced to the single integral

$$I = \int_{\mathcal{C}} \frac{F(q(\ell), s(\ell))}{|\nabla \gamma(q(\ell), s(\ell))|} \, \mathrm{d}\ell, \tag{B 2}$$

where $\ell$ is arclength along $\mathcal{C}$. (The result above assumes that in (B 1) $\eta \to 0$ through positive values: the sign is flipped if $\eta \to 0$ through negative values.)

To prove (B 2), note that in terms of intrinsic coordinates $(\ell, n)$

$$\mathrm{d}q \, \mathrm{d}s = \mathrm{d}\ell \, \mathrm{d}n = \frac{\mathrm{d}\ell \, \mathrm{d}\gamma}{|\nabla \gamma|}, \tag{B 3}$$

where $n$ is the normal distance from $\mathcal{C}$. Using (B 3) to convert (B 1) to a $(\gamma, \ell)$-integral and

$$\int_{-\infty}^{\infty} \frac{1}{\pi} \frac{\eta}{\gamma^2 + \eta^2} \, \mathrm{d}\gamma = 1, \tag{B 4}$$

to perform the integration over the coordinate $\gamma$, we obtain (B 2).

Now suppose that $\mathcal{C}$ is a graph and can therefore be parameterized as $s = f(q)$. The element of arclength is

$$\mathrm{d}\ell = \sqrt{1 + f'^2} \, \mathrm{d}q = \frac{|\boldsymbol{\nabla}\gamma|}{|\gamma_s|} \, \mathrm{d}q. \tag{B 5}$$

Thus, using $q$ to parameterize $\mathcal{C}$, the integral in (B 2) becomes

$$I = \int \frac{F(q, f(q))}{|\gamma_s(q, s(q))|} \, \mathrm{d}q. \tag{B 6}$$

## REFERENCES


BATTJES, J. & VAN VLEDDER, G. 1984 Verification of Kimura's theory for wave group statistics. In *Proceedings of the 19th International Conference Coastal Engineering*, pp. 642–648. ASCE. https://doi.org/10.1061/9780872624382.044.

VAN DEN BREMER, T. S. & TAYLOR, P. H. 2015 Estimates of Lagrangian transport by surface gravity wave groups: the effects of finite depth and directionality. *J. Geophys. Res.* **120** (4), 2701–2722.

VAN DEN BREMER, T. S. & TAYLOR, P. H. 2016 Lagrangian transport for two-dimensional deep-water surface gravity wave groups. *Proc. R. Soc. Lond.* A **472** (2192), 20160159.

CHELTON, D. B., DESZOEKE, R. A., SCHLAX, M. G., EL NAGGAR, K. & SIWERTZ, N. 1998 Geographical variability of the first baroclinic rossby radius of deformation. *J. Phys. Oceanogr.* **28** (3), 433–460.

ELGAR, S., GUZA, R. & SEYMOUR, R. 1984 Groups of waves in shallow water. *J. Geophys. Res.* **89** (C3), 3623–3634.

LAMB, H. 1932 *Hydrodynamics*. Cambridge University Press.

LIGHTHILL, M. 1967 On waves generated in dispersive systems to travelling forcing effects, with applications to the dynamics of rotating fluids. *J. Fluid Mech.* **27** (4), 725–752.

LIGHTHILL, M. 1978 *Waves in Fluids*. Cambridge University Press.

LONGUET-HIGGINS, M. S. & STEWART, R. 1964 Radiation stresses in water waves; a physical discussion, with applications. *Deep-Sea Res.* **11** (4), 529–562.

MCINTYRE, M. 1981 On the 'wave momentum' myth. *J. Fluid Mech.* **106**, 331–347.

OLBERS, D. J. & EDEN, C. 2016 Revisiting the generation of internal waves by resonant interaction with surface waves. *J. Phys. Oceanogr.* **46** (5).

OLBERS, D. J. & HERTERICH, K. 1979 The spectral energy transfer from surface waves to internal waves. *J. Fluid Mech.* **92** (02), 349–379.

PHILLIPS, O. M. 1977 *The Dynamics of the Upper Ocean*. Cambridge University Press.

PINKEL, R. 1975 Upper ocean internal wave observations from flip. *J. Geophys. Res.* **80** (27), 3892–3910.

WATSON, K. M., WEST, B. J. & COHEN, B. I. 1976 Coupling of surface and internal gravity waves: a mode coupling model. *J. Fluid Mech.* **77** (01), 185–208.